Available online at www.sciencedirect.com

ScienceDirect

journal homepage: http://www.elsevier.com/locate/acme

Original Research Article

# Prediction of average surface roughness and formability in single point incremental forming using artificial neural network

*Amrut Mulay* [a,*], *B. Satish Ben* [b], *Syed Ismail* [b], *Andrzej Kocanda* [c]

[a] *Mechanical Engineering Department, Indian Institute of Technology, Bombay 400076, India*
[b] *Mechanical Engineering Department, National Institute of Technology, Warangal 506004, India*
[c] *Faculty of Management and Computer Modeling, Kielce University of Technology, 25-314 Kielce, Poland*

ARTICLE INFO

*Article history:*
Received 10 December 2018
Received in revised form
22 April 2019
Accepted 2 June 2019
Available online 21 June 2019

*Keywords:*
Surface roughness
Formability
Artificial neural network
Incremental forming
Measurement

ABSTRACT

Single point incremental forming (SPIF) is a flexible, innovative, and cheap process for rapid manufacturing of complex sheet metal parts. It is a crucial task for engineers to predict a process when many independent parameters are affecting simultaneously its performance. An artificial neural network (ANN) based prediction model was developed to evaluate average surface roughness ($R_a$) and maximum forming angle ($Ø_{max}$) while SPIF forming of AA5052-H32 material. A feedforward backpropagation network with Levenberg–Marquardt algorithm was employed to build ANN model. The ANNs (4-*n*-1, 4-*n*-2) were generated by introducing different combinations of transfer functions and a number of neurons. The confirmation runs were performed to verify the agreement between the ANN predicted and the experimental results. The developed ANN model (4-*n*-1) was capable of predicting the process response with an excellent accuracy and resulted in overall *R*-value, MSE, and MAPE of 0.99807, 0.0209, and 5.96% for $R_a$ 0.99913, 0.0281, and 0.003 for $Ø_{max}$. The optimum 4-*n*-2 model was built with overall *R*-value, MSE of 0.99999 and 0.057194, respectively. Hence, it was found that the engineering efforts may be reduced in the SPIF process with successful ANN model implementation.



## 1. Introduction

Conventional forming has some disadvantages such as high capital cost, lower flexibility, and formability due to which incremental sheet forming (ISF) becomes a more popular process in the area of automotive, marine and aerospace, etc. According to the number of contact points, there are two types of ISF process such as single point incremental forming (SPIF) and two point incremental forming (TPIF). SPIF is a novel, versatile and cost effective process to form complex geometries. This forming technology is based on the localized plastic

* *Corresponding author.*
E-mail addresses: amrutmulay8@gmail.com, amrutmulay8@iitb.ac.in (A. Mulay), satishben@nitw.ac.in (B.S. Ben), syedismail7@nitw.ac.in (S. Ismail), andrzej.kocanda@gmail.com (A. Kocanda).
https://doi.org/10.1016/j.acme.2019.06.004
1644-9665/

deformation by the tool on the sheet metal. The rapid prototyping, customized product, new product development, short production time, etc. are the major requirements for fast moving competitive markets. The unit cost of the product has been significantly reduced in the case of small batch production due to the elimination of dedicated dies [1,2]. On the other hand, it has few disadvantages like less profile accuracy, higher production time and small batch production etc. The most of the sheet part is unconstraint during the forming which causes inaccuracy in the resulting component as well as hemispherical tool causes waviness on the sheet surface at higher step depth. The shearing and stretching of the sheet during incremental forming causes sheet thinning which can be approximated by sine's law [3]. The thinning behavior depends on imposed forming angle, and hence, the formability is defined by a maximum forming angle that sheet material would endure without fracturing. In SPIF, the sheet metal is clamped at four edges with the help of fixture on CNC machining center and tool movement is controlled with the help of CAD/CAM software. The machine control unit regulates the tool movement along the horizontal $x$–$y$ direction as well as gradual movement along the $z$ direction. The point by point movement of the tool path causes small local deformation at the vicinity of contact area and thus enhances overall formability. The ball ended tool forces the sheet metal to achieve the predefined shape. Recently, SPIF has gained significant attention in the manufacturing sector.

In the past, many researchers made efforts for minimizing drawbacks in SPIF process, and they tried to make this technology suitable to meet industrial purposes. For instance, Ambrogio et al. [4] proposed ANN implementation for the prediction of the height of specimen in the SPIF process taking into account geometrical variability. They compared error back propagation (EBP) and Levenberg–Marquardt (LM) algorithm to predict material failure in complex shapes. The result shows that LM method can predict the maximum height of deformed specimen more efficiently than EBP model. Liu et al. [5] investigated SPIF process with RSM's Box–Behnken design and multiobjective function. The impact of most influencing forming parameters such as sheet thickness, feed rate, tool diameter and step down was studied, and they found that sheet thickness is the most influential forming variable on the overall surface finish, followed by step depth. Durante et al. [6] performed an experimental work to deepen the knowledge of incremental forming. They investigated AA7075T0 under four different tool sheet contact types, and output characteristics such as surface roughness, forming force and formability, were studied. Azevedo et al. [7] studied about the influence of lubricants used during the SPIF forming of aluminum 1050 and DP780 steel sheets. They found that the use of a suitable lubricant can significantly improve surface quality, reduce forming forces and prevent tool wear. Ham and Jeswiet [8] studied SPIF process using the Box–Behnken method with five factors at three levels such as material type, material thickness, formed shape, tool size, and incremental step size. Cerro et al. [9] investigated the incremental forming process by experimental and finite element approach and process responses such as thickness distribution, geometrical inaccuracy, and surface roughness. Shanmuganatan and Senthil Kumar [10] deformed the sheet metal to understand the processing mechanism. They studied maximum wall angle, surface roughness and thinning of the sheet. In addition to this, metallurgical study and FEM simulation were also carried out. Golabi and Khazaali [11] used one factor at a time methodology to find the achievable depth of frustums made from SS304 with various cone angles, thicknesses, and major diameters. Cui et al. [12] showed that strain distribution has excellent co-relation in incremental sheet forming by comparing analytical, numerical and experimental techniques. They used a hyperbolic, skew and elliptical type of cone in their research. Bambach et al. [13] proved that multistage forming along with stress relief annealing before trimming could successfully improve the geometrical accuracy than single stage forming process. Attanasio et al. [14] performed experimental evaluation and optimization of tool path to form a part with best dimensional accuracy, best surface finish, and lowest sheet thinning. Kim and Park [15] studied the effect of process parameters such as tool type, tool size, feed rate, interface friction and plane anisotropy of the sheet on the formability of SPIF process. Shim and Park [16] demonstrated that crack occurs mostly at the corners due to greater deformation than that along a side. Mugendiran et al. [17] optimized surface roughness and sheet thickness of ISF using three influencing parameters such as spindle speed, tool feed, and step size. Minutolo et al. [18] performed experimental and numerical investigation for the evaluation of maximum wall angle in the case of pyramidal and cone frustums of aluminum alloy 7075T0 sheets. Mirnia et al. [19] compared SPIF process with sequential limit analysis and the explicit FE based model. They found that sequential limit analysis has better capability in predicting thickness distribution much closer to the experimental values than equivalent FE model. Duflou et al. [20] concluded that local heating at the contact zone leads to reduction in the force, unwanted deformation, and geometric errors. Park and Kim [21] investigated incremental forming on the complex geometries under various forming conditions. They proved that ISF gives better formability as compared to conventional forming techniques. Hussain et al. [22] carried out the formability investigation of an aluminum sheet under various radius of curvature of a part's generatrix, and they concluded that the formability increases when curvature radius decreases. Bhattacharya et al. [23] used Box–Behnken method for surface roughness study. They observed that formability of Al5052 sheet decreases with increase in tool diameter, incremental depth, and a decrease in sheet thickness while the surface roughness decreases with increase in tool diameters, increase in wall angle. The surface roughness increases first with an increase in incremental depth up to certain angle and then decreases. Riadh et al. [24] found that wall inclination angle and initial sheet thickness are the most influential parameters affecting sheet thinning and maximum punching load in SPIF process. Liu et al. [25] performed experimental campaign to evaluate successful part height, maximum draw angle, total forces during the incremental forming of AA7075-O. They found that SPIF formability is significantly affected by part draw angle and inclination depth of the tool path. In addition, they also concluded that the maximum vertical force increases as the step-down size and sheet thickness increases. Ziren et al. [2] used SPIF process for forming a U-shaped channel from

AA3003O sheets in order to verify the accuracy between flat end and hemispherical end tools. They concluded that the flat end tools provide better profile accuracy than the hemispherical end tools. Kurra and Regalla [26] carried out a comparative study between varying wall angle conical and pyramidal frustum with circular, elliptical, parabolic, and exponential generatrix. They found that conical frustums are under plane strain condition while pyramidal frustum experiences biaxial stretching. In addition to this; they also modeled SPIF process using different techniques such as artificial neural networks, support vector regression, and genetic programming. They initially optimized the process by using Box–Behnken design using independent model variables such as tool diameter, step depth, wall angle, feed rate and lubricant [27]. Gulati et al. [28] successfully optimized the formability and surface roughness during single point incremental forming of aluminum 6063 alloys based on Taguchi's $L_{18}$ orthogonal array. Palumbo and Brandizzi [29] investigated the effect of electric static heating and tool rotation speed on the incremental forming of Ti6Al4V sheets. Mulay et al. [30] studied the effect of SPIF process variables such as feed rate, step depth, tool diameter and sheet thickness on surface roughness and formability using response surface methodology. Honarpisheh et al. [31] performed experimental and numerical study of Al1050/Cu bimetal formed with SPIF process. The multiobjective optimization was carried out with fracture depth and wall thickness as response variable using RSM approach. Finally, they evaluated reaction force, thickness variation and stress distribution using FE analysis at optimum condition. Liu and Li [32] carried out comprehensive investigation of bimetallic roll bonded Cu-Al composite sheet. The study reveals that Al/Cu layer arrangement leads to higher formability and larger forming force compared to Cu/Al layer arrangement as the exterior thinner but stronger Cu layer could endure more stretching deformation. Kumar and Gulati [33] performed experimental investigation to study the effect of input parameters such as sheet thickness, tool diameter, step size, wall angle, feed rate, tool shape, oil viscosity and spindle speed on the surface roughness during incremental forming.

From the previous literature it has been found that, the SPIF performance is greatly affected by forming process parameters (step depth, tool rotational speed, feed rate, type of lubrication), material properties (stiffness, percentage elongation, strain hardening) and part geometrical parameters (wall angle, sheet thickness, type of wall curvature). A large scale research has been done by many researchers to know the process mechanics and improve the fundamental knowledge for better understanding. There are numerous research works published on process improvement for aluminum, steel, and titanium alloy materials. After an extensive literature survey, although a significant research was reported based on analytical, experimental and numerical techniques, no such an attempted has been made for predicting the surface quality and formability in the incremental forming of sheets. To fill this gap, in the present paper the plan of forty experiments was performed, and output responses were measured for each trial. It consists of various novelties such as (a) the artificial neural network models were developed to predict responses by considering key operating parameters, viz. feed rate ($f$), step depth ($p$), tool diameter ($d$), and sheet thickness ($t_o$); (b) all possible ANN architectures were implemented; (c) the effect of number of neurons in the hidden layer on response prediction capability. The good surface quality and higher formability are the major concerns for a commercialization of ISF technology into the industry. Furthermore, the principal goal of this research is to find most accurate ANN models without performing expensive experimental runs. It is necessary to understand the SPIF behavior when a process is dependent on multiple input process parameters. The objective of work also includes confirmation of ANN predicted results by performing additional experiments.

## 2. Experimental procedures and materials

The experiments were performed at Indo-German Tool Room, Aurangabad, India. The current work was carried out on varying wall angle conical frustum (VWACF) with circular generatrix. Incremental sheet forming (ISF) experiments were carried out using a three axis computerized numerical control (CNC) vertical milling machine within the working range of input process factors and the corresponding average surface roughness ($R_a$) and maximum forming angle ($Ø_{max}$) were recorded.

### 2.1. *Experimental conditions and plan*

The SPIF forming fixture have been mounted on CNC machine bed (Model: Surya VF 30 CNC VS, Make: Bharat Fritz Werner LTD, Bangalore, India) as shown in Fig. 1. The SPIF forming is carried out on various thicknesses (0.8 mm, 1 mm, and 1.2 mm) of AA5052 H32 alloy sheets of dimensions 222 mm × 222 mm with the help of a hemispherical tool. The forming tool was perfectly fastened into the collect chuck as shown in Fig. 1. The surface hardened high-speed steel (62–65 HRC) hemispherical tools of 8 mm, 10 mm and 12 mm in diameters were utilized in the investigation. The continuous series of small plastic local deformations were carried out with

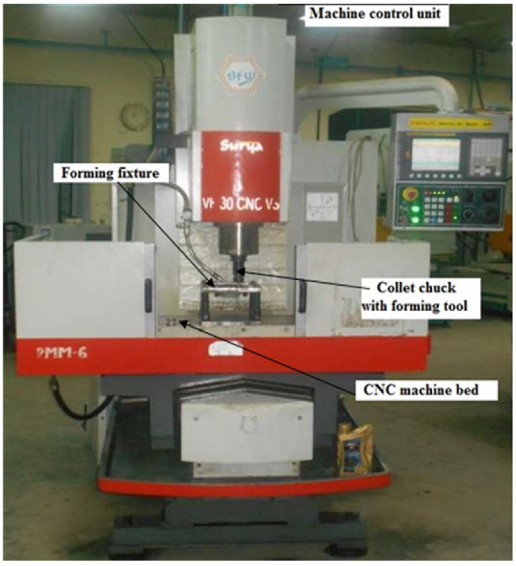


**Fig. 1 – Experimental setup for single point incremental forming process on CNC milling machine.**

the help of a tool. During the forming, each point on the contour experiences elasto-plastic loading and unloading. The tools were finely polished by different grades of abrasive papers. The forming fixture composed of the top plate, backing plate, vertical columns, and bottom plate. The backing plate with center orifice was placed below the sheet in order to easy flow of material and prevents the bending of the sheet during initial forming. In the process, the movement of the tool with respect to sheet metal is controlled by machine control unit along x, y, and z-directions. In the trial experiments, it has been observed that performance parameters of SPIF are enhanced by applying oil lubricant at tool sheet interface. It was also observed that an increase in tool rotation speed and table feed rate lead to high amount of frictional heat and burning of lubricant which further causes early sheet fracture. Therefore, Castrol 10W30 synthetic mineral oil is used as a lubricant as it shows very good results while incremental forming of aluminum alloys [7]. The oil of a viscosity of 71.5 $mm^2/s$ at 40 °C, the relative density of 0.856 g/ml at 15 °C.

The varying wall angle conical frustum (VWACF) geometry was chosen in SPIF investigation. The commercial CAD/CAM software such as UG-NX CAM 8.5 was used for designing 3D geometry and generating tool path. Fig. 2(a) indicates the development of tool path using CAM software based upon CAD geometry. The Z-level profile tool path was adopted to generate clockwise circular contour followed by vertical step depth ($p$) between each consecutive contour. After the completion of each contour, the tool moves down at certain depth called step depth and further traces next contour of slightly lower diameter than the previous contour. Before the start of forming, the flatness of the blank was measured and then adjusted with the help of dial gauge indicator with least count of 0.001 mm.

The dimensions of cone are as follows: initial wall angle ($Ø_i$) = 30°, final wall angle ($Ø_f$) = 90°, major radius of cone ($r_i$) = 69 mm, minor radius of cone ($r_f$) = 34 mm, radius of circular generatrix ($r$) = 70 mm and total height of the cone ($h$) = 60.62 mm. The dimensions of the VWACF are shown in Fig. 2(b). In the previous literature study, it was observed that formability decreased at higher step depth, feed rate, and tool rotational speed. The higher thinning of sheet leads to fracture. It has been well understood that the thickness of the sheet decreases along the specimen depth. The reduction in sheet thickness leads to instability point in the material which causes crack initiation. The angle at which material breaks due to high concentrated stresses in tool sheet interface is called as maximum forming angle i.e. $Ø_{max}$. The higher thinning rate has been observed to be associated with shallow parts or part with lesser maximum forming angle [11]. The variations in the $R_a$ and $Ø_{max}$ depend on inputs of the incremental forming process. The angle at any arbitrary fractured point can be found out by Eq. (1),

The forming angle at point c,

$$\emptyset_c = \cos^{-1}\left(\frac{y_c}{r}\right) = \cos^{-1}\left(\frac{h_t - h_p}{r}\right) \tag{1}$$

In Eq. (1), total sample height ($h_t$) and radius of circular generatrix ($r$) are the known parameters while $h_p$ is the height of formed part from $P_i$ ($x_i$, $y_i$). The Taylor-Hobson Surtronic S-100 series profilometer was used to measure $R_a$. The final $R_a$ value was determined by taking an average of three

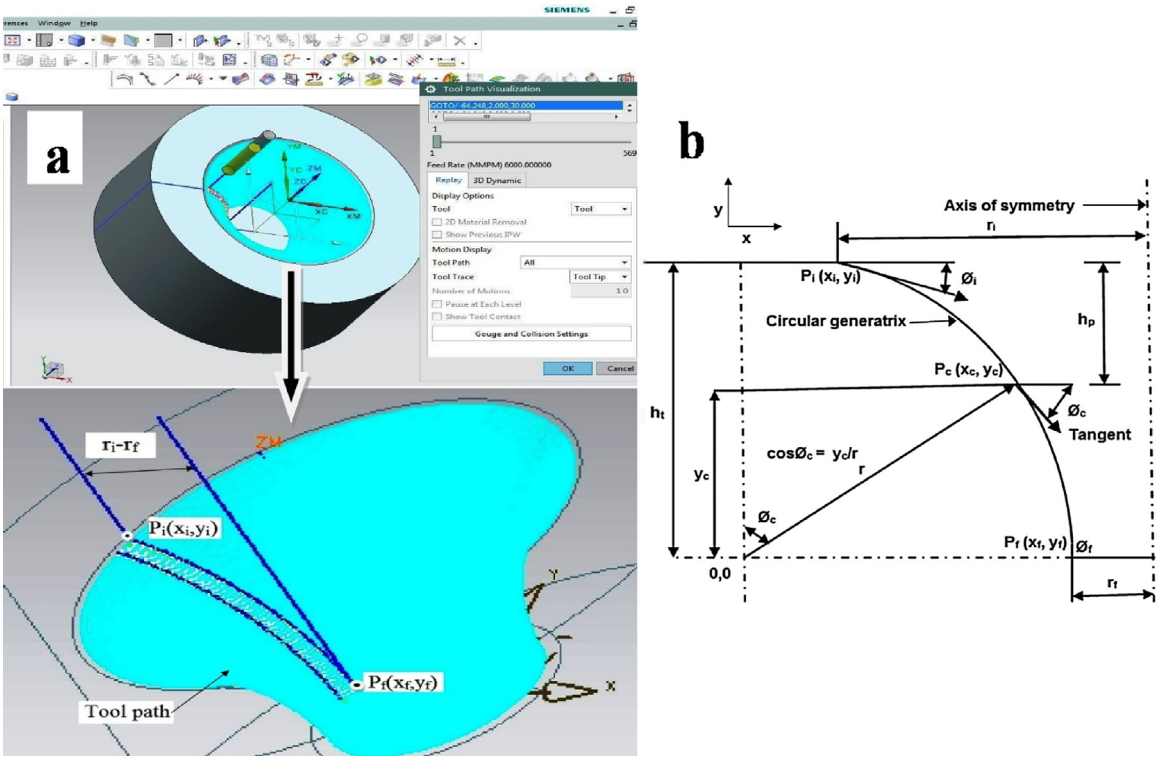


**Fig. 2 – SPIF process: (a) development of contour path from CAM software, (b) geometrical details of a specimen.**

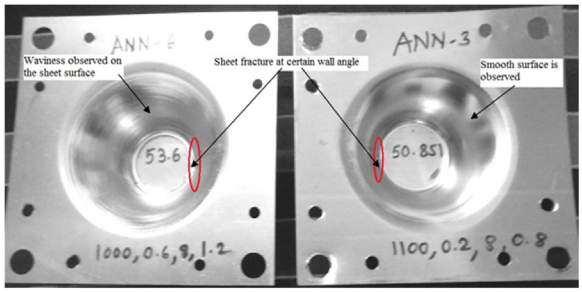


**Fig. 3 – The sample specimens resulting from SPIF at different process condition.**

measurements with a sampling length ($L_c$) of 2.5 mm. It is an arithmetic mean of deviation of the profile from the center line along sampling length. The best capacity of used surface roughness tester is ±(2% + 0.004 μm). The surface roughnesses of formed sheets were measured at three different locations along the step depth direction at the inner side of the sheet surface. Three forming tests were performed to ensure the reproducibility of the results. It is always desirable to form the product with the higher forming angle and lower $R_a$. The sample specimens produced from SPIF process are shows in Fig. 3. It indicates the change in the $R_a$ and formability at two different combinations of process parameters.

### 2.2. *Material*

Interest in the utilization of aluminum alloys has been developed due to the production of lightweight vehicles with high fuel economy. As per AA 5xxx alloys, magnesium is a major alloying element with aluminum. The Al-Mg alloy shows high corrosive resistance, non-heat treatable, high strength properties. The AA5052 H32 alloy can replace existing material in order to reduce a weight of the system by introducing thinner sheets at the same strength level. The mechanical properties of the material were confirmed by the tensile test as per ASTM E8 standards in the directions of 0°, 45°, and 90° to the rolling direction and the properties of AA5052 H32 are as follows: yield strength of 189.53 MPa, ultimate tensile strength of 260.37 MPa, the maximum elongation of 12.23%. The AA5052 H32 sheet has chemical composition of 2.5, Mg; 0.26, Cr; 0.13, Si; 0.33, Fe; 0.08, Cu; 0.06, other; (balance) Al was considered for investigation [34]. Since Al-Mg alloys have high strength, low weight properties, and high formability, these alloys can be utilized in aerospace and automotive industries.

The parameters and their levels were selected based on previous literature, machine capabilities and pilot experiments. The one-factor-at-a-time was used to evaluate the effect of each process parameter on the process performance. The suitable working range of process parameters was selected in the present study. Table 1 shows the independent parameters and their respective levels to evaluate the SPIF performance. The goal of this investigation is to generate a best ANN prediction model to form the sheet metal without any defects such as higher surface roughness, extra material thinning, material failure, etc.

## 3. Response surface methodology

The Design of Experiment is used to organize the experimental run in order to get a fruitful outcome. Response surface methodology (RSM) is a widely used statistical tool to carry out systematic set of experiments. RSM is a collection of mathematical and statistical techniques useful for the modeling and analysis of problems in which a response of interest is influenced by several variables. The input parameters and their levels were defined after the pilot experimental study of each factor using one-factor-at-a-time. RSM answers the question of how to select process parameters to obtain the desirable value of the response with a reduced number of experiments. The behavior of the response with the changes in the variables can be represented by the surface not a curve, thus, a response surface methodology is needed. One of the most applicable and prosperous RSM's tools is Box–Behnken. In this design, the process parameter combinations are at the midpoints of edges of the process space and at the center [30]. These designs are rotatable (or near rotatable). The design matrix was built considering four input parameters (feed rate, step depth, tool diameter, and sheet thickness) at three levels. This could be advantageous when the points on the corners of the cube represent factor- level combinations that are prohibitively expensive or impossible to test due to physical process constraints. The 29 data sets were generated according to single block Box–Behnken design with four factors at three levels. However, for developing good ANN model, a higher number of data is required. Therefore, additionally, 11 data sets were generated randomly within the range of input process parameters. Three specimens were prepared at same forming condition of design matrix in order to minimize noise (forming error) and corresponding responses were recorded during the SPIF process (Table 2).

**Table 1 – Independent process parameters and their levels.**

| Parameter | Unit | Coded process parameters | | |
|---|---|---|---|---|
| | | −1 | 0 | 1 |
| Feed rate ($f$) | mm/min | 600 | 1400 | 2200 |
| Step depth ($p$) | mm | 0.2 | 0.4 | 0.6 |
| Tool diameter ($d$) | mm | 8 | 10 | 12 |
| Sheet thickness ($t_o$) | mm | 0.8 | 1 | 1.2 |

**Table 2 – The SPIF input and corresponding response variable data in the ANN model.**

| Runs | Feed rate (mm/min) | Step depth (mm) | Tool diameter (mm) | Sheet thickness (mm) | Surface roughness (μm) | Maximum forming angle (°) |
|---|---|---|---|---|---|---|
| 1 | 600 | 0.2 | 10 | 1 | 2.1 | 83.9 |
| 2 | 2200 | 0.2 | 10 | 1 | 2.3 | 83.45 |
| 3 | 600 | 0.6 | 10 | 1 | 4.2 | 80.8 |
| 4 | 2200 | 0.6 | 10 | 1 | 4.5 | 77.38 |
| 5 | 1400 | 0.4 | 8 | 0.8 | 4.8 | 82.68 |
| 6 | 1400 | 0.4 | 12 | 0.8 | 2.8 | 77.54 |
| 7 | 1400 | 0.4 | 8 | 1.2 | 4.2 | 82.56 |
| 8 | 1400 | 0.4 | 12 | 1.2 | 2.6 | 78.35 |
| 9 | 600 | 0.4 | 10 | 0.8 | 3.3 | 80 |
| 10 | 2200 | 0.4 | 10 | 0.8 | 3.5 | 78.98 |
| 11 | 600 | 0.4 | 10 | 1.2 | 3.2 | 82.33 |
| 12 | 2200 | 0.4 | 10 | 1.2 | 3.3 | 79.95 |
| 13 | 1400 | 0.2 | 8 | 1 | 3.3 | 85.06 |
| 14 | 1400 | 0.6 | 8 | 1 | 7.7 | 80.34 |
| 15 | 1400 | 0.2 | 12 | 1 | 1.9 | 81.51 |
| 16 | 1400 | 0.6 | 12 | 1 | 3.5 | 76.26 |
| 17 | 600 | 0.4 | 8 | 1 | 5.4 | 81.72 |
| 18 | 2200 | 0.4 | 8 | 1 | 5.9 | 80.69 |
| 19 | 600 | 0.4 | 12 | 1 | 2.9 | 78.36 |
| 20 | 2200 | 0.4 | 12 | 1 | 3.2 | 77.35 |
| 21 | 1400 | 0.2 | 10 | 0.8 | 2.4 | 83.45 |
| 22 | 1400 | 0.6 | 10 | 0.8 | 4.7 | 77.96 |
| 23 | 1400 | 0.2 | 10 | 1.2 | 2.1 | 83.11 |
| 24 | 1400 | 0.6 | 10 | 1.2 | 4.2 | 81.87 |
| 25 | 1400 | 0.4 | 10 | 1 | 3.2 | 81.2 |
| 26 | 1400 | 0.4 | 10 | 1 | 3.2 | 81.2 |
| 27 | 1400 | 0.4 | 10 | 1 | 3.2 | 81.2 |
| 28 | 1400 | 0.4 | 10 | 1 | 3.2 | 81.2 |
| 29 | 1400 | 0.4 | 10 | 1 | 3.2 | 81.2 |
| 30 | 1400 | 0.6 | 8 | 1.2 | 6.9 | 82.2 |
| 31 | 1400 | 0.2 | 10 | 1 | 2.15 | 83.95 |
| 32 | 1400 | 0.4 | 12 | 1 | 2.75 | 78.6 |
| 33 | 1400 | 0.4 | 8 | 1 | 5.4 | 82.3 |
| 34 | 600 | 0.4 | 12 | 1.2 | 2.6 | 79.44 |
| 35 | 2200 | 0.2 | 12 | 0.8 | 2.55 | 81 |
| 36 | 600 | 0.6 | 12 | 0.8 | 3.48 | 75.1 |
| 37 | 2200 | 0.2 | 10 | 0.8 | 2.43 | 83.6 |
| 38 | 2200 | 0.6 | 10 | 1.2 | 4.77 | 78.2 |
| 39 | 600 | 0.2 | 8 | 1 | 3.45 | 84.35 |
| 40 | 600 | 0.6 | 10 | 1.2 | 4.25 | 82.57 |

## 4. Topology, structure and artificial development of neural networks

The ANN is most powerful and simple modeling technique based on statistical techniques which do not require any kind of mathematical model. The complex non-linear relationship between independent inputs and responses can be easily predicted by neural network soft computing tool which is due to the inspiration of biological nervous systems and functioning of the human brain. The neural network architecture consists of the input layer, hidden layer, and an output layer. All nodes of subsequent layers are connected to each other and neurons in a hidden layer were varied. The input layer receives the information from an external source, which is subsequently multiplied by the interconnection weights between it and the adjacent hidden layer and then the products are summed up. The summation of the product is further modified by transfer functions, and these modified values will be an output of first hidden layer and input for the next layer. In this way, the signal reaches to an external receptor node(s) or output layer. By achieving the learning ability, ANN produces the desired responses according to the given decision variables [35]. The ANN optimization is carried out on 'nnstart' wizard of MATLAB R2014a software (The Mathworks Inc., Massachusetts, USA). The steps involved in search of optimum neural network model have been illustrated in Fig. 4. Topology and structure of the artificial neural system are shown in Figs. 5–7. Finding the ANN topology with best network configurations is the most important step in neural network modeling. Four independent process parameters such as $f$, $p$, $d$, $t_o$ are considered in the input layer while $R_a$, $\emptyset_{max}$ are considered in the output layer of ANN modeling. The neural networks were developed for predicting $R_a$ and $\emptyset_{max}$ individually.

At the start of the development stage, the process treatment combinations and output responses are fed to Matlab software as input and target data, respectively. The different networks are created based on a number of neurons

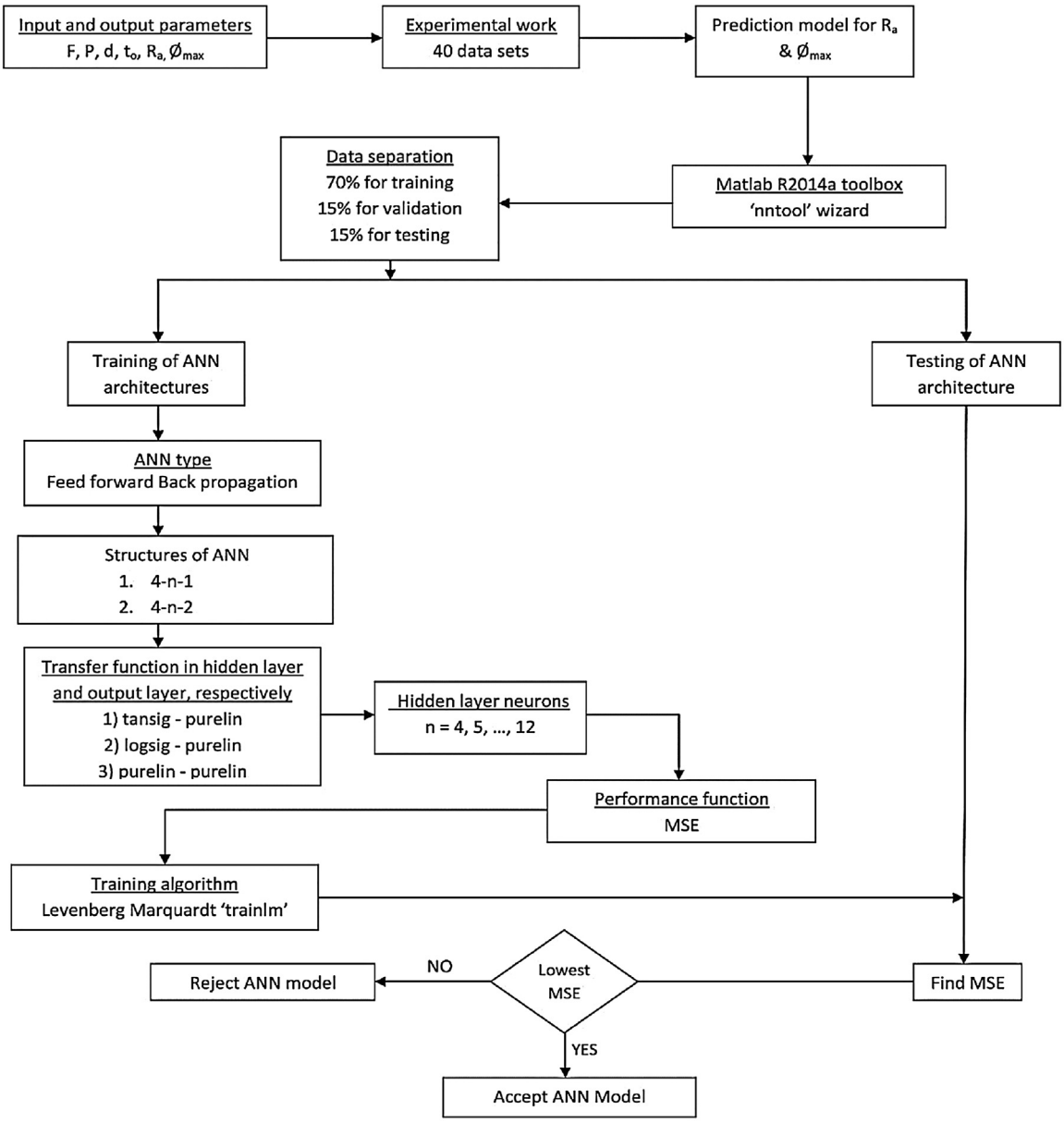


**Fig. 4 – Step involved in the search of optimum neural network in present investigation.**

in the hidden layer and type of transfer function at each layer. Levenberg–Marquardt algorithm (trainlm) is used to initialize the new weight, bias values and train the network for better optimization. It is the most commonly used algorithm which offers the best generalization and easy convergence in less number of iterations [36]. The training is aimed at minimizing the error by adjusting the weights of the network. Suppose a function $V(x)$ is to be minimized with respect to parameter vector $_x$, then Newton's method would be

$$\Delta_x = -[\nabla^2 V(_x)]^{-1} \nabla V(_x) \tag{2}$$

In Eq. (2), $\nabla^2 V(_x)$ is the Hessian matrix of the error function at particular weights and biases and $\nabla V(_x)$ is the gradient of an error function. It is assumed that $V(_x)$ is the sum of square function and is expressed by Eq. (3),

$$V(x) = \sum_{i=1}^{N} e_i^2(_x) \tag{3}$$

Eq. (4) reveals Marquardt–Levenberg modification to the Gauss–Newton method and it can be mathematically represented as,

$$\Delta_x = [J^T(_x) J(_x) + \mu I]^{-1} J^T(_x) e(_x) \tag{4}$$

The key step in this algorithm is the computation of Jacobean matrix (i.e., $J(_x)$) by a simple modification to back propagation algorithm. The parameter $\mu$ is multiplied by some factor ($\beta$) if a step would result in an increased $V(_x)$ and is divided by $\beta$ if a step would result in decrease in $V(_x)$. The direction in which the search is performed is described by a single iteration of an algorithm which is shown in Eq. (5).

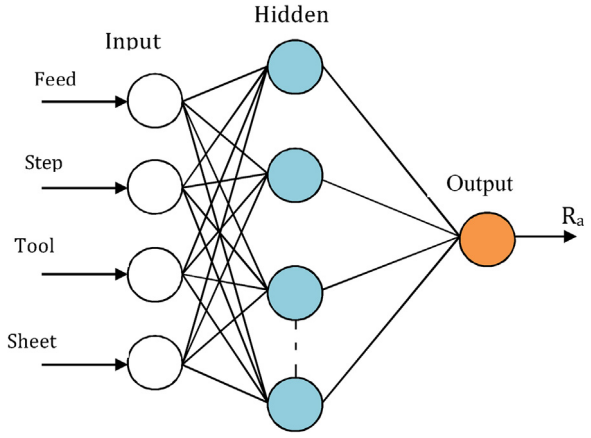


**Fig. 5 – The structure of ANN (4-*n*-1) for average surface roughness.**

$$x_{k+1} = x_k - [J^T(x)J(x) + \mu I]^{-1} J^T(x) e(x) \quad (5)$$

The LM is an approximation to the Newton's method and well suited to the training of the neural architecture [4]. By this algorithm, the improvement in the performance of the neural network in terms of a sum of square error value and epochs required to train the network were found to be reduced. In all the developed neural networks adaptation learning function and performance function are employed as LEARNGD and MSE respectively. According to number of parameters in input and output layer, the following two types of architecture were studied,

1. The 4-*x*-1 topology (Figs. 5 and 6) is selected in the modeling of neural networks where, 4 indicates number of neurons in the input layer ($f$, $p$, $d$, $t_o$), '*x*' indicates number of neurons in the hidden layer, 1 indicates number of neurons in the output layer ($R_a$ or $\emptyset_{max}$).
2. The 4-*x*-2 topology (Fig. 7) is similar to 4-*x*-1 except for number of neurons in the output layer. '<!– no-mfc –>2'<!– /no-mfc –> indicate the output layer neurons ($R_a$ and $\emptyset_{max}$).

In order to determine the optimal architecture, the trial-and-error approach is carried out by adjusting the number of neurons in the hidden layer. The correct number of neurons has to be selected to avoid over-fitting due to more neurons and under fitting due to fewer neurons. The number of neurons in the hidden layer gradually increases from 4 to 12 and effect on the predicted response is recorded. Nine different neural networks such as (4-4-1, 4-5-1, 4-6-1, 4-7-1, 4-8-1, 4-9-1, 4-10-1, 4-11-1, 4-12-1) are developed by varying number of neurons in the hidden layer. The similar procedure was adopted in the case of 4-*x*-2 topology. During modeling, the hyperbolic tangent sigmoid function 'tansig,' log sigmoid transfer function 'logsig,' and pure linear function 'purelin' have been utilized as the transfer function. The tansig and logsig transfer functions can be calculated by Eqs. (6) and (7), respectively.

$$\text{tansig}(n) = \frac{2}{1+e^{-2n}} - 1 \quad (6)$$

$$\text{logsig}(n) = \frac{1}{1+e^{-n}} \quad (7)$$

To have a good correlation between predicted and target values, the pure linear transfer function (purelin) is always defined for the output layer [37]. Out of overall data the 70% of the total data were used for training, 15% for validation, and 15% for testing [38]. Therefore, 28 data were used for training, 6 data for validation, and 6 data for testing. Since the result of the training phase majorly depends on the initialization of the interconnection weights and sampling of data, each ANN was trained five times. Confirmation of ANN results with target

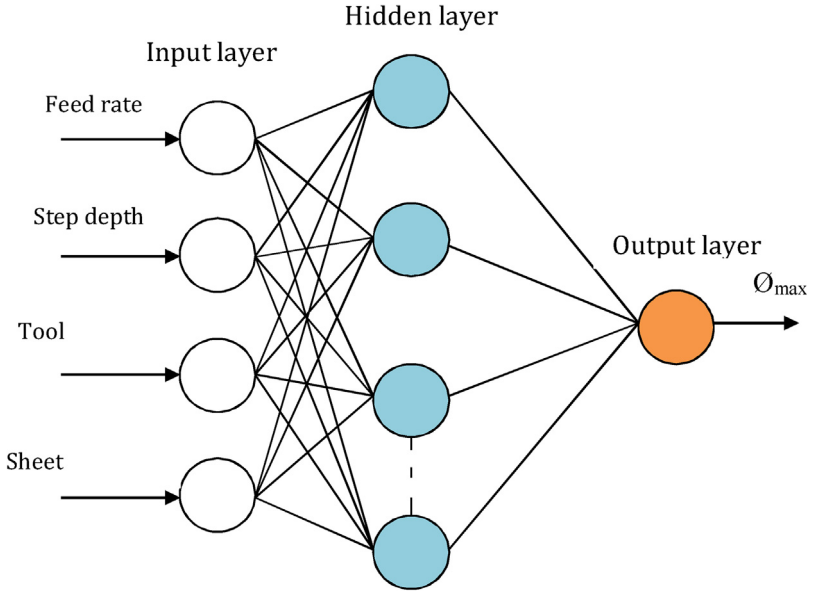


**Fig. 6 – The structure of ANN (4-*n*-1) for maximum forming angle.**

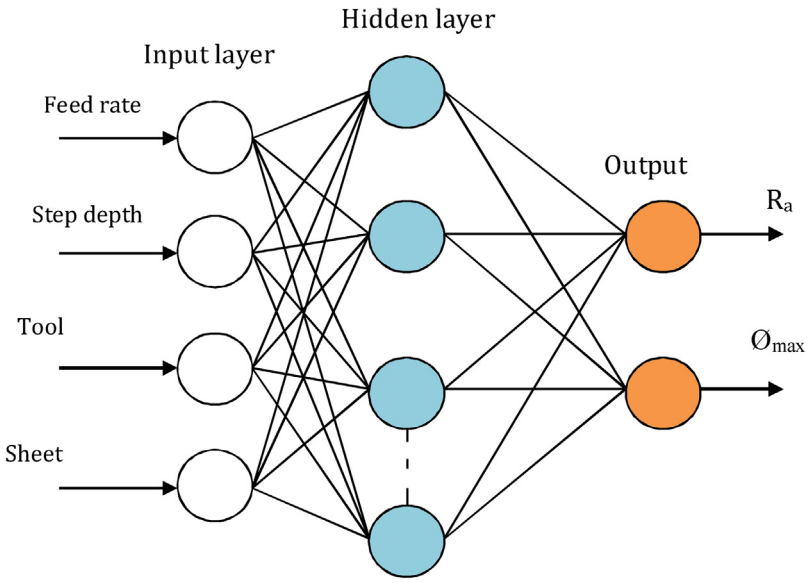


**Fig. 7 – The structure of ANN (4-*n*-2) for two output neurons i.e. average surface roughness and maximum forming angle.**

values is carried out by employing a new input data set which was not used in training. After the training is over, the network generates an output file for all the predicted responses for given input treatments. In addition to this, one more file is generated which accounts an error between predicted and target values.

### 4.1. *Feed forward back propagation network*

The multilayer feed forward back propagation (FFBP) with three transfer functions (tangent sigmoid transfer function, log sigmoid transfer function, pure linear transfer function) are selected for a hidden layer of ANN. Data obtained from experimental factors i.e. $f$, $p$, $d$, $t_o$, $R_a$, $\emptyset_{max}$ are provided to a neural network in the learning stage. The network learning is done to minimize the difference between predicted and the target value. If the difference is quite large, then the connector weights initialize to a new value, and network predicts another output. The error is propagated backward till it reaches an acceptable value. During the ANN architecture, the number of neurons in the hidden layer and type of transfer function for each layer are the critical design parameters.

### 4.2. *Mathematical representation of neural networks*

The hidden layer includes several processing units connected with variable weights called neurons. Each neuron is connected to another neuron with a certain weight in the network. An input signal $x_j$ connected to neuron $k$ is multiplied by the synaptic weight $w_{kj}$. The processing of neural network has been mathematically expressed by Eqs. (8) and (9),

$$u_k = \sum_{j=1}^{m} (w_{kj} \times x_j) \tag{8}$$

$$y_k = f(u_k + b_k) \tag{9}$$

where, $x_1, x_2, \ldots, x_m$ are input signals; $w_{k1}, w_{k2}, \ldots, w_{km}$ are the synaptic weights of neuron $k$; $u_k$ is linear combiner due to the input signals; $b_k$ is the bias; $f$ is the activation function; and $y_k$ is the output signal of the neuron.

During the learning stage, predicted output is compared with target output, and the connector weights inside the network are adjusted to minimize the difference. The network forecasts the output according to the knowledge it has gained. The training of a network is completed when the validation error starts to increase in order to avoid over learning of network and corresponding mean squared error (MSE) value was noted. The performance of a neural network is evaluated by MSE and coefficient of correlation ($R$ value) [34]. The co-relationship is said to be strong if the predicted and target values are very close to the line for the entire datasets. The good ANN architecture is selected based on lower MSE and higher $R$ values. The minimization of MSE was carried out by updating the weights through gradient descent method. The MSE value can be found out by Eq. (10),

$$\text{MSE} = \frac{1}{N}\sum_{i=1}^{N} (y_{pi} - y_{ti})^2 \tag{10}$$

where $y_{pi}$ and $y_{ti}$ are network prediction and a target values for ith observation respectively, $N$ is the total number of observations. The $R$ value is used to show a relationship between predicted and random values. The relationship is said to be close if $R$ value is nearly equal to ''1'' while the relationship is said to be random if $R$ value is nearly equal to ''0''.

## 5. Results and discussion

In the paper, the various neural network models were developed based on a number of neurons in the hidden layer and type of transfer functions. The modeling of SPIF process is

carried out with the help of feed forward back propagation ANN network architecture. Figs. 5–7 show the schematic representation of an artificial neural network to predict $R_a$ and $Ø_{max}$. To get a good fit model, the various possible combinations of transfer functions and gradually increasing the number of neurons in the hidden layer is utilized in this investigation. A deviation of predicted results from experimental results is given in the form of mean absolute percentage error (MAPE) [38–40]. It can be formulated by the following Eq. (11),

$$\text{MAPE} = \frac{1}{N}\sum_{i=1}^{N}\left(\left|\frac{y_{pi}-y_{ti}}{y_{ti}}\right|\right)\times 100 \tag{11}$$

### 5.1. *ANN model for the individual response ($R_a$ or $Ø_{max}$)*

In this study, an attempt has been made to formulate a prediction model between key SPIF process parameters and requested response variable. The three neural network based models were developed by considering a different number of neurons and three different combinations of transfer functions. These models revealed accuracy to different degrees. Table 3 reflects the R value and MSE for $R_a$ prediction model '3-*n*-<!– no-mfc –>1'<!– /no-mfc –> when trained by using FFBP network and Levenberg–Marquardt algorithm. It is observed that lowest average MSE value is obtained with ten neurons in the hidden layer. The network 4-10-1 gives highest *R* value of 0.99807 and lowest MSE value of 0.0291 out of all the ANN models, and the results inferred that the neural network with ten neurons with a tangent sigmoid transfer function in the hidden layer can predict an $R_a$ closer to the observed target value. In the optimum ANN model for the $R_a$, the tansig and pureline transfer functions were employed in the hidden and output layer, respectively. The corresponding *R* values for training, testing and validation were 0.99699, 0.99851, and 0.99884, respectively. The *R* value lies between 0 and 1. If it is 1, then it shows perfect correlation, and in a case of 0, it implies no relationship between predicted and actual response. The trained network was tested again for additional data, and corresponding MAPE was calculated. The lowest value of MAPE is expected from optimum ANN network. Fig. 10(a) shows the relation between the predicted and target $R_a$ values by performing confirmation experiments. The mean error was calculated based on the results of trial experiments in order to verify the practical suitability of developed ANN model. It has been observed that MAPE is found to be 5.97% and the $R^2$ value of 0.973. Hence, the 4-10-1 ANN model is confident enough to forecast the responses for unknown input process variables.

Table 4 shows the *R*-value and MSE in predicting $Ø_{max}$ for SPIF forming process by the 3-*n*-1 model that is trained by Levenberg–Marquardt algorithm with FFBP type of network. The network 4-9-1 gives the highest *R*-value of 0.99913 and

**Table 3 – Summary of trial and error method for prediction of $R_a$ using 4-*n*-1 ANN model.**

| Hidden layer neurons | Transfer function | | R values | | | | MSE |
|---|---|---|---|---|---|---|---|
| | Layer 1 | Layer 2 | Training | Testing | Validation | All | |
| 4 | TANSIG | PURELIN | 0.99599 | 0.99127 | 0.99086 | 0.99085 | 0.109 |
| 5 | | | 0.99822 | 0.94621 | 0.95633 | 0.98941 | 0.118 |
| 6 | | | 0.99397 | 0.96501 | 0.99407 | 0.98981 | 0.05 |
| 7 | | | 0.99752 | 0.98026 | 0.92947 | 0.98373 | 0.1589 |
| 8 | | | 1 | 0.9535 | 0.98566 | 0.99734 | 0.0488 |
| 9 | | | 1 | 0.96447 | 0.95523 | 0.97966 | 0.1943 |
| **10** | | | **0.99699** | **0.99851** | **0.99884** | **0.99807** | **0.0209** |
| 11 | | | 0.9999 | 0.98033 | 0.95716 | 0.98262 | 0.2802 |
| 12 | | | 0.99999 | 0.96939 | 0.9911 | 0.98841 | 0.2176 |
| 4 | LOGSIG | PURELIN | 0.99809 | 0.9875 | 0.90347 | 0.98166 | 0.1709 |
| 5 | | | 0.99917 | 0.97899 | 0.95501 | 0.98993 | 0.1449 |
| 6 | | | 0.99608 | 0.97639 | 0.95696 | 0.99133 | 0.0409 |
| 7 | | | 0.99578 | 0.98875 | 0.90908 | 0.99231 | 0.0399 |
| 8 | | | 0.99716 | 0.90341 | 0.99045 | 0.98947 | 0.0502 |
| 9 | | | 0.99867 | 0.91403 | 0.98491 | 0.99649 | 0.037 |
| 10 | | | 0.9999 | 0.95016 | 0.99096 | 0.99184 | 0.0428 |
| 11 | | | 0.99683 | 0.95063 | 0.93303 | 0.98052 | 0.213 |
| 12 | | | 0.99726 | 0.98006 | 0.94373 | 0.98384 | 0.1237 |
| 4 | PURELIN | PURELIN | 0.90687 | 0.96223 | 0.99032 | 0.91156 | 0.1451 |
| 5 | | | 0.90599 | 0.94878 | 0.95155 | 0.91187 | 0.1335 |
| 6 | | | 0.92019 | 0.9439 | 0.96901 | 0.91112 | 0.145 |
| 7 | | | 0.90485 | 0.92672 | 0.99667 | 0.9108 | 0.1719 |
| 8 | | | 0.90529 | 0.92068 | 0.95955 | 0.91138 | 0.0908 |
| 9 | | | 0.9115 | 0.92418 | 0.96319 | 0.91094 | 0.0929 |
| 10 | | | 0.90662 | 0.94263 | 0.97013 | 0.91189 | 0.179 |
| 11 | | | 0.90563 | 0.90967 | 0.95908 | 0.91177 | 0.1524 |
| 12 | | | 0.9038 | 0.93619 | 0.93725 | 0.9109 | 0.2673 |

MSE: mean square error, FFBP: feed forward back propagation, TANSIG: tangent sigmoid transfer function, LOGSIG: log sigmoid transfer function, PURELIN: linear transfer function. Bold values refer to the best values.

**Table 4 – Summary of trial and error method for prediction of $Ø_{max}$ (i.e. formability) using 4-*n*-1 ANN model.**

| Hidden layer neurons | Transfer function | | R values | | | | MSE |
|---|---|---|---|---|---|---|---|
| | Layer 1 | Layer 2 | Training | Testing | Validation | All | |
| 4 | TANSIG | PURELIN | 0.99859 | 0.9148 | 0.97839 | 0.97586 | 0.5819 |
| 5 | | | 0.99766 | 0.96545 | 0.96117 | 0.98499 | 0.4442 |
| 6 | | | 0.9991 | 0.99701 | 0.99643 | 0.99162 | 0.17326 |
| 7 | | | 0.99442 | 0.96677 | 0.94984 | 0.98239 | 0.4008 |
| 8 | | | 0.99416 | 0.92889 | 0.97261 | 0.98167 | 0.2423 |
| **9** | | | **0.9995** | **0.99924** | **0.99648** | **0.99913** | **0.0281** |
| 10 | | | 0.9982 | 0.81999 | 0.9689 | 0.987 | 0.3195 |
| 11 | | | 0.99997 | 0.92912 | 0.9839 | 0.98577 | 0.1633 |
| 12 | | | 0.99996 | 0.98666 | 0.92301 | 0.97722 | 1.048 |
| 4 | LOGSIG | PURELIN | 0.97734 | 0.93575 | 0.98654 | 0.97191 | 0.4189 |
| 5 | | | 0.99975 | 0.92716 | 0.97281 | 0.98501 | 0.4428 |
| 6 | | | 0.99618 | 0.95673 | 0.94306 | 0.98884 | 0.2355 |
| 7 | | | 0.99954 | 0.96558 | 0.96223 | 0.98337 | 0.4841 |
| 8 | | | 1 | 0.97983 | 0.99568 | 0.99481 | 0.1035 |
| 9 | | | 1 | 0.99577 | 0.9545 | 0.97974 | 1.4747 |
| 10 | | | 0.99116 | 0.97769 | 0.95861 | 0.98629 | 0.2656 |
| 11 | | | 0.99615 | 0.99931 | 0.97748 | 0.97364 | 0.7268 |
| 12 | | | 1 | 0.97832 | 0.90949 | 0.97095 | 1.2447 |
| 4 | PURELIN | PURELIN | 0.89387 | 0.90736 | 0.91021 | 0.88986 | 1.0138 |
| 5 | | | 0.85965 | 0.94703 | 0.98103 | 0.89557 | 1.2943 |
| 6 | | | 0.89842 | 0.92706 | 0.90416 | 0.89413 | 1.2287 |
| 7 | | | 0.86834 | 0.9198 | 0.96006 | 0.89377 | 0.9297 |
| 8 | | | 0.86459 | 0.92397 | 0.97347 | 0.89543 | 1.0487 |
| 9 | | | 0.91686 | 0.843 | 0.8506 | 0.89652 | 1.0638 |
| 10 | | | 0.89611 | 0.92495 | 0.9368 | 0.89629 | 1.2074 |
| 11 | | | 0.86877 | 0.96827 | 0.97738 | 0.89642 | 1.0185 |
| 12 | | | 0.87592 | 0.92799 | 0.89041 | 0.89058 | 1.0103 |

MSE: mean square error, FFBP: feed forward back propagation, TANSIG: tangent sigmoid transfer function, LOGSIG: log sigmoid transfer function, PURELIN: linear transfer function. Bold values refer to the best values.

lowest MSE value of 0.0281, and the results inferred that the neural network with nine neurons in the hidden layer with tangent sigmoid transfer function predicts the $Ø_{max}$ closer to the observed target value. In the optimum ANN model for the $Ø_{max}$, the tansig and pureline transfer functions were employed in the hidden and output layer, respectively. The *R* values for training, validation, and testing were 0.9995, 0.99924, and 0.99648, respectively. The mean error was calculated based on trial experiments in order to verify the practical suitability of developed ANN model. Fig. 10(b) shows the predicted vs. actual response of $Ø_{max}$ with MAPE of 0.3% and the $R^2$ value of 0.955. Hence, the 4-9-1 ANN model is confident enough to forecast the responses for unknown input process variables.

From the discussion on the results of different models, done so far, it is determined that the tansig and purelin transfer functions in hidden and output layer, respectively are recommendable since they revealed the lowest average MSE in the case of $R_a$ and $Ø_{max}$.

### 5.2. *ANN model for two responses in the output layer ($R_a$ and $Ø_{max}$)*

In the study, Figs. 8 and 9 and Table 5 illustrate the best capability of 4-7-2 NN model in predicting $R_a$ and formability together with log sigmoid transfer function. The *R*-value is reported to be 0.99999, MSE of 0.05719 which is an indication of good fit. It is the lowest value of MSE over the all investigated neural networks in a present study. The *R* values of 1, 0.99994, and 0.99998 corresponding to training, testing, and validation, respectively. The logsig is found to be more efficient than tansig and purelin transfer functions to get accurate ANN structure with two neurons in the output layer.

Fig. 10(c, d) reveals that the $R^2$ and MAPE are found to be 94.2% and 8.1521%, respectively in case of $R_a$ whereas it is 0.927 and 0.769% for $Ø_{max}$, respectively. The results showed an

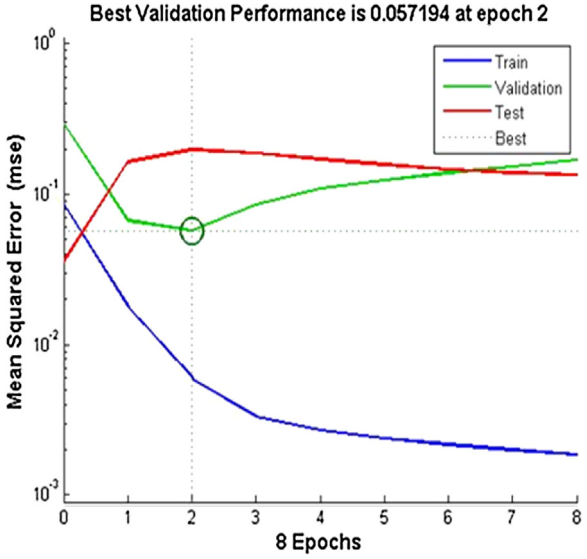


**Fig. 8 – Performance plot at 4-7-2 (logsig-purelin) network model.**

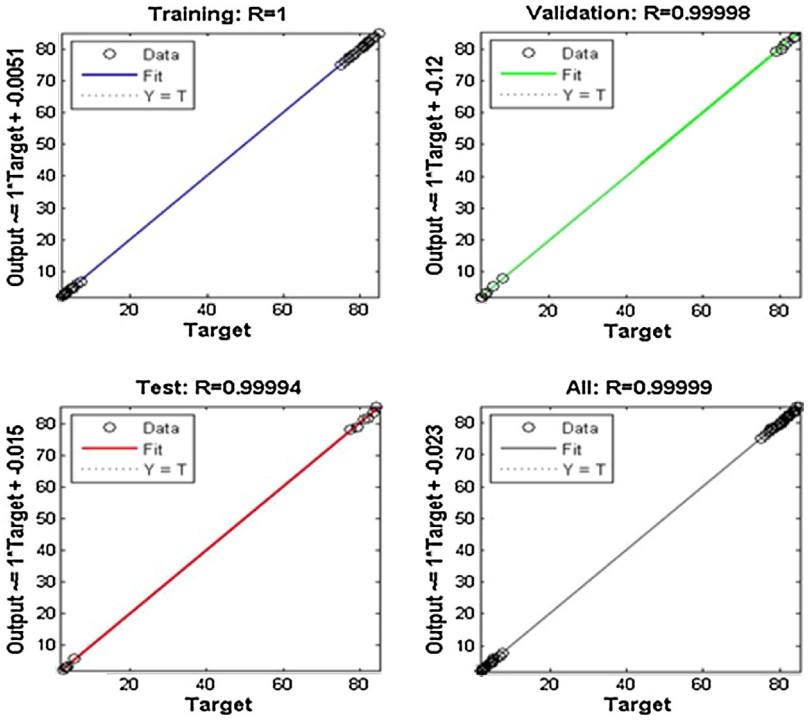


**Fig. 9 – Regression plot of 4-7-2 (logsig-purelin) network model (training, testing, and validation).**

**Table 5 – Summary of trial and error method for prediction of $R_a$ and $Ø_{max}$ (i.e. formability) simultaneously using 4-*n*-2 ANN model.**

| Hidden layer neurons | Transfer function | | R values | | | | MSE |
|---|---|---|---|---|---|---|---|
| | Layer 1 | Layer 2 | Training | Testing | Validation | All | |
| 4 | TANSIG | PURELIN | 0.99985 | 0.99961 | 0.99982 | 0.9998 | 0.6988 |
| 5 | | | 0.99987 | 0.9998 | 0.99989 | 0.99983 | 0.467 |
| 6 | | | 0.99997 | 0.99997 | 0.99994 | 0.99996 | 0.2127 |
| 7 | | | 1 | 0.99965 | 0.99988 | 0.99992 | 0.4076 |
| 8 | | | 0.99996 | 0.99981 | 0.99986 | 0.99992 | 0.4173 |
| 9 | | | 1 | 0.99962 | 0.99985 | 0.99989 | 0.4845 |
| 10 | | | 0.99985 | 0.99984 | 0.99987 | 0.99983 | 0.4533 |
| 11 | | | 0.99989 | 0.99954 | 0.99979 | 0.99981 | 0.7473 |
| 12 | | | 0.99985 | 0.99941 | 0.99966 | 0.99975 | 1.0513 |
| 4 | LOGSIG | PURELIN | 0.99993 | 0.99992 | 0.99994 | 0.99993 | 0.1935 |
| 5 | | | 0.99998 | 0.99935 | 0.9998 | 0.99982 | 0.5694 |
| 6 | | | 0.9999 | 0.99992 | 0.99982 | 0.99989 | 0.5627 |
| **7** | | | **1** | **0.99994** | **0.99998** | **0.99999** | **0.0572** |
| 8 | | | 0.99997 | 0.99933 | 0.99969 | 0.99979 | 1.3523 |
| 9 | | | 1 | 0.99973 | 0.99981 | 0.99989 | 0.653 |
| 10 | | | 0.99991 | 0.99991 | 0.9999 | 0.99991 | 0.3091 |
| 11 | | | 0.99988 | 0.99958 | 0.99962 | 0.99979 | 1.2252 |
| 12 | | | 0.9999 | 0.99998 | 0.9999 | 0.99991 | 0.2953 |
| 4 | PURELIN | PURELIN | 0.99975 | 0.99993 | 0.99964 | 0.99975 | 1.2993 |
| 5 | | | 0.99982 | 0.99969 | 0.99959 | 0.99977 | 1.2815 |
| 6 | | | 0.99984 | 0.99964 | 0.99956 | 0.99974 | 1.33 |
| 7 | | | 0.99982 | 0.99985 | 0.99978 | 0.99977 | 1.2081 |
| 8 | | | 0.99976 | 0.99989 | 0.99962 | 0.99975 | 1.2256 |
| 9 | | | 0.99976 | 0.99995 | 0.99962 | 0.99976 | 1.1757 |
| 10 | | | 0.99978 | 0.99985 | 0.99957 | 0.99976 | 1.2638 |
| 11 | | | 0.9998 | 0.99962 | 0.9996 | 0.99974 | 1.2563 |
| 12 | | | 0.99978 | 0.99989 | 0.99959 | 0.99976 | 1.2415 |

MSE: mean square error, FFBP: feed forward back propagation, TANSIG: tangent sigmoid transfer function, LOGSIG: log sigmoid transfer function, PURELIN: linear transfer function. Bold values refer to the best values.

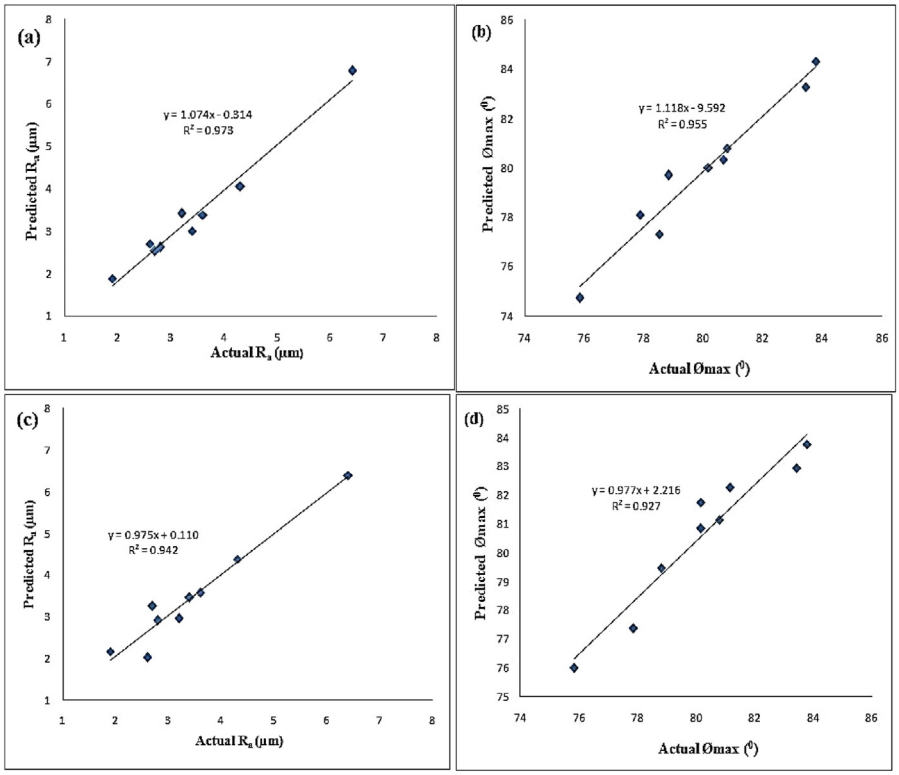


**Fig. 10 – ANN prediction vs. actual response data (a) 4-*n*-1 model of surface roughness (b) 4-*n*-1 model of maximum forming angle (c) 4-*n*-2 model of surface roughness (d) 4-*n*-2 model of maximum forming angle.**

excellent co-relationship between input and output parameters and generated ANN model can predict the output with the higher confidence level for a new set of inputs.

## 6. Conclusions

In the present study, the key responses and process parameters such as table feed rate, step depth, tool diameter and sheet thickness of SPIF process were successfully modeled with feed forward back propagation method using the artificial neural network. The best-predicted model is selected after evaluating a large number of neural networks with different training functions and a number of neurons into the hidden layer. The following conclusions were made out of the investigation

1. The $R_a$ and $Ø_{max}$ are possible to control in single point incremental forming using developed neural network architecture.
2. The optimized neural network for predicting $R_a$ consist of tansig and pureline transfer functions in the hidden and output layer respectively with 10 number of neurons (4-10-1) while 9 number of neurons in the hidden layer (4-9-1) in the case of $Ø_{max}$. It was observed that overall R-value between predicted and target data is 0.99807 and 0.98913 in the case of $R_a$ and $Ø_{max}$, respectively indicating close relationship for the selected neural network model.
3. The developed 4-10-1 and 4-9-1 ANN networks are reliable to forecast $R_a$ and $Ø_{max}$ in the case of unexposed data with an absolute average percentage error of 5.97% and 0.3% respectively.
4. The 4-7-2 model with logsig (hidden layer)-purelin (output layer) transfer function is found to be appropriate for predicting $R_a$ and $Ø_{max}$ simultaneously for any specified combination of table feed, step depth, tool diameter and sheet thickness. The correlation coefficient of 0.99999, MSE of 0.05719 reflects an excellent relationship between input and output process variables.
5. The validity of neural network is confirmed by the additional experiments. The confirmation results show that the ANN predictions are in good agreement with experimental results.

It has been inferred that the responses of this study were effectively predicted by ANN. The huge economical benefits, higher predictability, short simulation time make ANN to be a promising modeling tool as demonstrated here. This could benefit to a forming industry, particularly research and development phase where cost and time reduction is a major objective.

## Funding

Ministry of Human Resource Development, Government of India and Warsaw University of Technology, Poland.

## Acknowledgements

The authors are thankful to Department of Mechanical Engineering, National Institute of Technology, Warangal for its continuous support toward carrying out research work and resolving necessary financial issues under Ministry of Human Resource Development, Government of India as well as to Department of Metal Forming and Casting, Faculty of Production Engineering, Warsaw University of Technology, Poland.

## REFERENCES

[1] G. Buffa, D. Campanella, L. Fratini, On the improvement of material formability in SPIF operation through tool stirring action, Int. J. Adv. Manuf. Technol. 66 (2013) 1343–1351.
[2] X. Ziran, L. Gao, G. Hussain, Z. Cui, The performance of flat end and hemispherical end tools in single-point incremental forming, Int. J. Adv. Manuf. Technol. 46 (2010) 1113–1118.
[3] G. Hussain, L. Gao, Z.Y. Zhang, Formability evaluation of a pure titanium sheet in the cold incremental forming process, Int. J. Adv. Manuf. Technol. 37 (2008) 920–926.
[4] G. Ambrogio, L. Filice, F. Guerriero, R. Guido, D. Umbrello, Prediction of incremental sheet forming process performance by using a neural network approach, Int. J. Adv. Manuf. Technol. 54 (2011) 921–930.
[5] Z. Liu, S. Liu, Y. Li, P. Meehan, Modelling and optimization of surface roughness in incremental sheet forming using a multi-objective function, Mater. Manuf. Process. 29 (2014) 808–818.
[6] M. Durante, a. Formisano, A. Langella, F.M. Capece Minutolo, The influence of tool rotation on an incremental forming process, J. Mater. Process. Technol. 209 (2009) 4621–4626.
[7] N.G. Azevedo, J.S. Farias, R.P. Bastos, P. Teixeira, J.P. Davim, R. J. Alves de Sousa, Lubrication aspects during single point incremental forming for steel and aluminum materials, Int. J. Precis. Eng. Manuf. 16 (2015) 589–595.
[8] M. Ham, J. Jeswiet, Single point incremental forming limits using a Box-Behnken design of experiment, Key Eng. Mater. 344 (2007) 629–636.
[9] I. Cerro, E. Maidagan, J. Arana, a. Rivero, P.P. Rodríguez, Theoretical and experimental analysis of the dieless incremental sheet forming process, J. Mater. Process. Technol. 177 (2006) 404–408.
[10] S.P. Shanmuganatan, V.S. Senthil Kumar, Experimental investigation and finite element modeling on profile forming of conical component using Al 3003(O) alloy, Mater. Des. 36 (2012) 564–569.
[11] S. Golabi, H. Khazaali, Determining frustum depth of 304 stainless steel plates with various diameters and thicknesses by incremental forming, J. Mech. Sci. Technol. 28 (2014) 3273–3278.
[12] Z. Cui, Z. Cedric Xia, F. Ren, V. Kiridena, L. Gao, Modeling and validation of deformation process for incremental sheet forming, J. Manuf. Process. 15 (2013) 236–241.
[13] M. Bambach, B. Taleb Araghi, G. Hirt, Strategies to improve the geometric accuracy in asymmetric single point incremental forming, Prod. Eng. 3 (2009) 145–156.
[14] A. Attanasio, E. Ceretti, C. Giardini, L. Mazzoni, Asymmetric two points incremental forming: improving surface quality and geometric accuracy by tool path optimization, J. Mater. Process. Technol. 197 (2008) 59–67.
[15] Y.H. Kim, J.J. Park, Effect of process parameters on formability in incremental forming of sheet metal, J. Mater. Process. Technol. 130–131 (2002) 42–46.
[16] M.S. Shim, J.J. Park, The formability of aluminium sheet in incremental forming, J. Mater. Process. Technol. 113 (2001) 654–658.
[17] V. Mugendiran, A. Gnanavelbabu, R. Ramadoss, Parameter optimization for surface roughness and wall thickness on AA5052 aluminium alloy by incremental forming using response surface methodology, Procedia Eng. 97 (2014) 1991–2000.
[18] F.C. Minutolo, M. Durante, A. Formisano, A. Langella, Evaluation of the maximum slope angle of simple geometries carried out by incremental forming process, J. Mater. Process. Technol. 193 (2007) 145–150.
[19] M.J. Mirnia, B. Mollaei Dariani, H. Vanhove, J.R. Duflou, Thickness improvement in single point incremental forming deduced by sequential limit analysis, Int. J. Adv. Manuf. Technol. 70 (2014) 2029–2041.
[20] J.R. Duflou, B. Callebaut, J. Verbert, H. De Baerdemaeker, Improved SPIF performance through dynamic local heating, Int. J. Mach. Tools Manuf. 48 (2008) 543–549.
[21] J.J. Park, Y.H. Kim, Fundamental studies on the incremental sheet metal forming technique, J. Mater. Process. Technol. 140 (2003) 447–453.
[22] G. Hussain, L. Gao, N. Hayat, L. Qijian, The effect of variation in the curvature of part on the formability in incremental forming: an experimental investigation, Int. J. Mach. Tools Manuf. 47 (2007) 2177–2181.
[23] A. Bhattacharya, K. Maneesh, N. Venkata Reddy, J. Cao, Formability and surface finish studies in single point incremental forming, J. Manuf. Sci. Eng. 133 (2011) 061020, http://dx.doi.org/10.1115/1.4005458.
[24] B. Riadh, A. Henia, B. Hedi, Application of response surface analysis and genetic algorithm for the optimization of single point incremental forming process, Key Eng. Mater. 557 (2013) 1265–1272.
[25] Z. Liu, Y. Li, P.A. Meehan, Experimental investigation of mechanical properties, formability and force measurement for AA7075-O aluminum alloy sheets formed by incremental forming, Int. J. Precis. Eng. Manuf. 14 (2013) 1891–1899.
[26] S. Kurra, S.P. Regalla, Experimental and numerical studies on formability of extra-deep drawing steel in incremental sheet metal forming, Integr. Med. Res. 3 (2014) 158–171.
[27] S. Kurra, N.H. Rahman, S.P. Regalla, A.K. Gupta, Modeling and optimization of surface roughness in single point incremental forming process, J. Mater. Res. Technol. 4 (2015) 304–313.
[28] V. Gulati, A. Aryal, P. Katyal, A. Goswami, Process parameters optimization in single point incremental forming, J. Inst. Eng. (India): Ser. C 97 (2015) 221–229.
[29] G. Palumbo, M. Brandizzi, Experimental investigations on the single point incremental forming of a titanium alloy component combining static heating with high tool rotation speed, Mater. Des. 40 (2012) 43–51.
[30] A. Mulay, S. Ben, S. Ismail, A. Kocanda, Experimental investigations into the effects of SPIF forming conditions on surface roughness and formability by design of experiments, J. Braz. Soc. Mech. Sci. Eng. (2017), http://dx.doi.org/10.1007/s40430-016-0703-7.
[31] M. Honarpisheh, M. Jobedar, M. Alinaghian, Multi-response optimization on single-point incremental forming of hyperbolic shape Al-1050/Cu bimetal using response surface methodology, Int. J. Adv. Manuf. Technol. 96 (2018) 3069–3080.
[32] G. Liu, Z. Li, Single point incremental forming of Cu-Al composite sheets: a comprehensive study on deformation behaviors, Arch. Civ. Mech. Eng. 19 (2019) (2019) 484–502.
[33] A. Kumar, V. Gulati, Experimental investigation and optimisation of surface roughness in negative incremental forming, Measurement 131 (2019) 419–430.
[34] S. Park, C.G. Lee, H.N. Han, S.-J. Kim, K. Chung, Improvement of the drawability based on the surface friction stir process of

AA5052-H32 automotive sheets, Met. Mater. Int. 14 (2008) 47–57.
[35] M. Mia, N. Ranjan, Prediction of surface roughness in hard turning under high pressure coolant using artificial neural network, Measurement 92 (2016) 464–474.
[36] M.T. Hagan, M.B. Menhaj, Training feedforward networks with the Marquardt algorithm, IEEE Trans. Neural Netw. 5 (1994) 2–6.
[37] M.R. Thakker, J.K. Parikh, M.A. Desai, Microwave assisted extraction of essential oil from the leaves of Palmarosa: multi-response optimization and predictive modelling, Ind. Crops Prod. 86 (2016) 311–319.
[38] A. Chakraborty, S. Roy, R. Banerjee, An experimental based ANN approach in mapping performance- emission characteristics of a diesel engine operating in dual-fuel mode with LPG, J. Nat. Gas Sci. Eng. 28 (2016) 15–30.
[39] T.T. Nguyen, Y.S. Yang, K.Y. Bae, S.N. Choi, Prediction of deformations of steel plate by artificial neural network in forming process with induction heating, J. Mech. Sci. Technol. 23 (2009) 1211–1221.
[40] S. Roy, R. Banerjee, A.K. Das, P.K. Bose, Development of an ANN based system identification tool to estimate the performance-emission characteristics of a CRDI assisted CNG dual fuel diesel engine, J. Nat. Gas Sci. Eng. 21 (2014) 147–158.